Electronic Supplementary Material (ESI) for Physical Chemistry Chemical Physics.

Approaching the free-ion limit in magnetically isotropic gadolinium(III) *via* borohydride ligands

Michał Magott*[a] and Wojciech Wegner*[b]

a) Faculty of Chemistry, Jagiellonian University, Gronostajowa 2, 30-387 Krakow, Poland.

b) Centre of New Technologies, University of Warsaw, ul. Banacha 2c, 02-097 Warszawa, Poland. E-mail: w.wegner@cent.uw.edu.pl; michal.magott@uj.edu.pl

S1. Results of Rietveld refinement

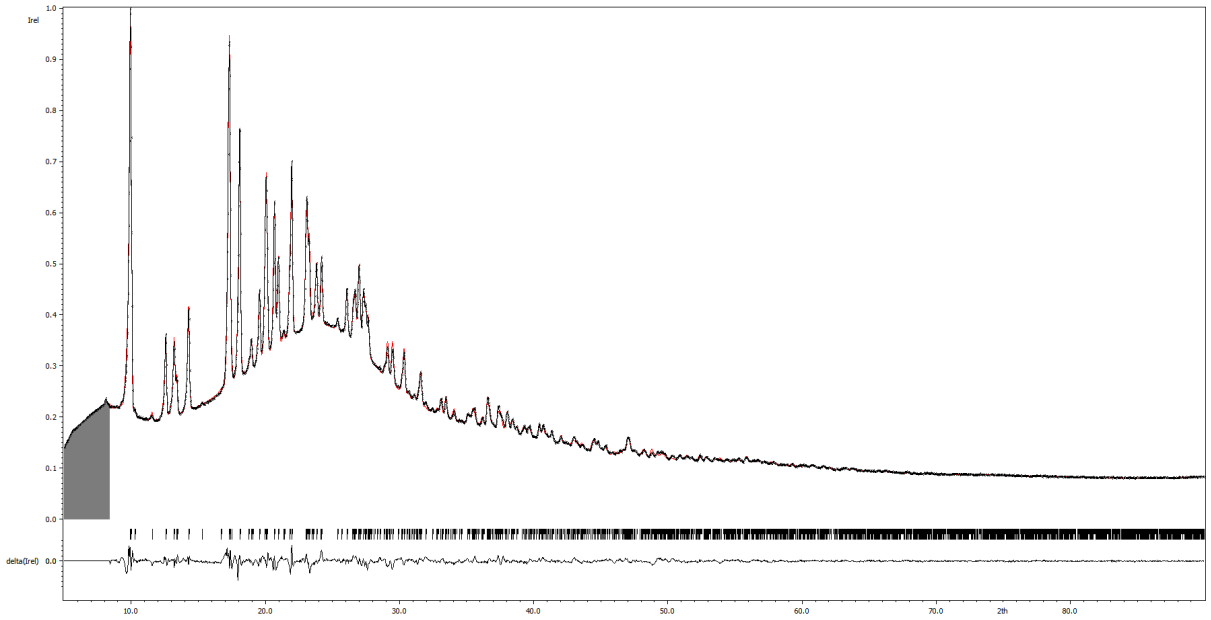

Figure S1. Rietveld refinement for sample containing only **1**. Experimental data are represented by a black curve, calculated profile by a red curve. The positions of the Bragg reflections are marked and the difference curve (between the experimental and calculated profiles) are plotted at the bottom figure. Excluded region: minor impurities from zeolitic molecular sieves used for drying the DCM.

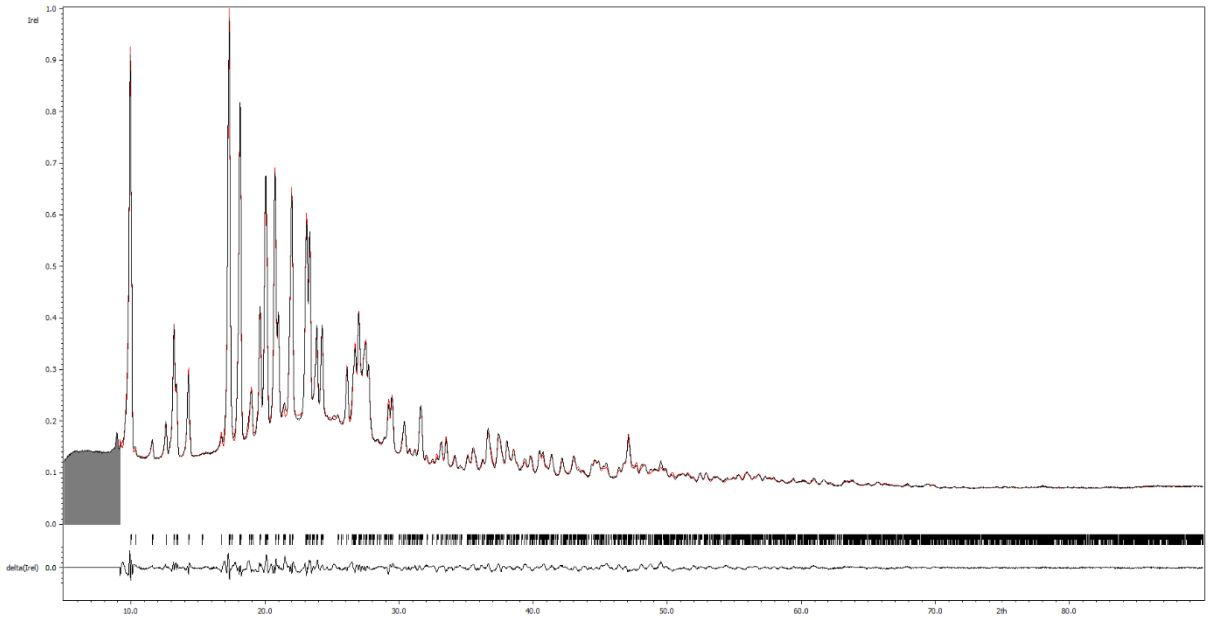

Figure S2. Rietveld refinement for sample containing only **2**. Experimental data are represented by a black curve, calculated profile by a red curve. The positions of the Bragg reflections are marked and the difference curve (between the experimental and calculated profiles) are plotted at the bottom figure. Excluded region: minor impurities from zeolitic molecular sieves used for drying the DCM.

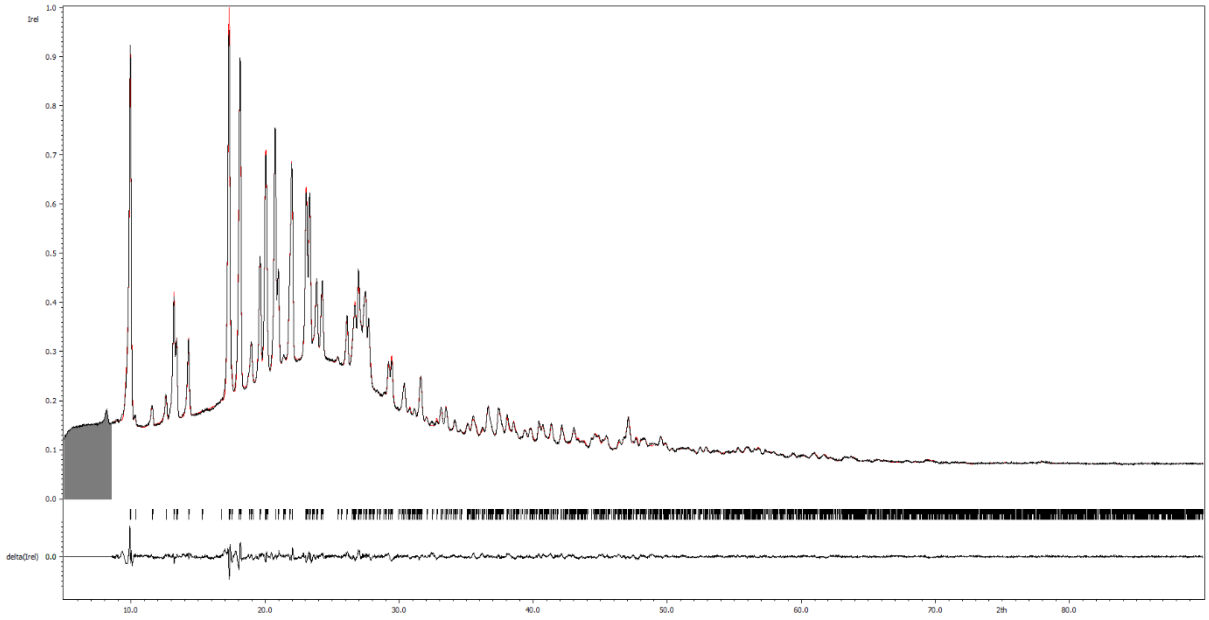

Figure S3. Rietveld refinement for sample containing only **3**. Experimental data are represented by a black curve, calculated profile by a red curve. The positions of the Bragg reflections are marked and the difference curve (between the experimental and calculated profiles) are plotted at the bottom figure. Excluded region: minor impurities from zeolitic molecular sieves used for drying the DCM.

Table S1. Comparison of the crystal structure parameters of known α-TBA*RE*$(BH_4)_4$ with gadolinium compounds obtained here.*

Ln	**Gd (1)**			**$Gd_{0.097}Y_{0.903}$ (2)**	**$Gd_{0.017}Y_{0.983}$ (3)**	**Dy**[1]	**$Dy_{0.1}Y_{0.9}$**[1]	**Y**[2]		**Ho**[3]		**Tm**[3]
RE^{3+} r[1] [Å]	0.938			0.938/0.900	0.938/0.900	0.912	0.912/0.900	0.900		0.901		0.880
space group	$P2_1/c$			$P2_1/c$	$P2_1/c$	$P2_1/c$	$P2_1/c$	$P2_1/c$		$P2_1/c$		$P2_1/c$
T [K]	DFT (0 K)	100	RT	RT	RT	RT	RT	100	RT	100	RT	RT
a [Å]	11.28150	11.0900(5)	11.4886(10)	11.4444(9)	11.4412(5)	11.4240(10)	11.4464(7)	11.0453(5)	11.4181(10)	11.039(3)	11.4218(9)	11.4063(18)
b [Å]	19.83197	19.9970(10)	20.590(3)	20.568(2)	20.5624(14)	20.531(2)	20.5665(17)	20.0099(9)	20.510(3)	19.999(2)	20.553(2)	20.545(4)
c [Å]	15.26347	14.7492(7)	15.3211(18)	15.3112(14)	15.3137(9)	15.2885(18)	15.3250(12)	14.7204(8)	15.2811(19)	14.708(4)	15.3049(17)	15.319(3)
β [°]	130.80281	128.282(1)	129.528(7)	129.446(6)	129.445(4)	129.478(8)	129.468(4)	127.980(5)	129.464(8)	128.02(4)	129.433(7)	129.423(12)
V [Å^3]	2585.0	2567.5(2)	2795.4(6)	2783.2(5)	2782.1(3)	2767.8(6)	2785.1(4)	2564.44	2762.77	2558.1(10)	2775.0(5)	2773.1(10)
Z	4			4	4	4	4	4		4		4

* Effective ionic radius (6-coordinate, octahedral environment) from ref. [4]

Table S2. Gd–Gd, Gd–B and Gd–H distances and B–Gd–B angles from **1** crystal structure obtained by SC-XRD at 100 K.

Distance	**1** (100 K)
shortest Gd···Gd	7.7784(6) Å 8.7949(6) Å 9.0640(5) Å
Gd1-B1	2.529(5) Å
Gd1-B2	2.533(5) Å
Gd1-B3	2.532(5) Å
Gd1-B4	2.522(5) Å
Gd1-H1B	2.30(5) Å
Gd1-H2B	2.33(4) Å
Gd1-H4B	2.33(4) Å
Gd1-H5B	2.28(5) Å
Gd1-H6B	2.36(5) Å
Gd1-H7B	2.32(5) Å
Gd1-H9B	2.26(5) Å
Gd1-H10B	2.26(5) Å
Gd1-H11B	2.32(5) Å
Gd1-H13B	2.32(5) Å
Gd1-H14B	2.30(5) Å
Gd1-H15B	2.32(5) Å
Angle	
B1-Gd1-B2	107.43(17)°
B1-Gd1-B3	108.32(18)°
B1-Gd1-B4	109.43(16)°
B2-Gd1-B3	110.31(18)°
B2-Gd1-B4	111.87(16)°
B3-Gd1-B4	109.39(17)°

Table S3. RE–RE, RE–B and RE–H distances and B–RE–B angles from **1-3** crystal structures obtained by PXRD at RT.

Distance	**1** (RT)	**2** (RT)	**3** (RT)
shortest RE···RE	8.123(9) Å 9.270(8) Å 9.34(4) Å 9.73(4) Å	8.128(7) Å 9.258(7) Å 9.30(3) Å 9.68(3) Å	8.133(6) Å 9.259(5) Å 9.34(2) Å 9.62(2) Å
RE-B1	2.48(9) Å	2.66(8) Å	2.46(7) Å
RE-B2	2.48(11) Å	2.26(12) Å	2.42(8) Å
RE-B3	2.49(6) Å	2.44(10) Å	2.13(7) Å
RE-B4	2.47(4) Å	2.48(5) Å	2.42(4) Å
RE-H2_b	2.36(19) Å	2.51(14) Å	2.34(7) Å
RE-H3_b	2.3(6) Å	2.5(5) Å	2.3(4) Å
RE-H4_b	2.3(3) Å	2.52(14) Å	2.33(14) Å
RE-H6_b	2.36(18) Å	2.4(3) Å	2.31(13) Å
RE-H7_b	2.35(12) Å	2.37(12) Å	2.30(11) Å
RE-H8_b	2.35(14) Å	2.3(3) Å	2.32(18) Å
RE-H10_b	2.37(12) Å	2.34(16) Å	2.06(13) Å
RE-H11_b	2.3(4) Å	2.3(4) Å	2.0(4) Å
RE-H12_b	2.37(15) Å	2.34(9) Å	2.05(8) Å
RE-H14_b	2.36(5) Å	2.2(3) Å	2.3(4) Å
RE-H15_b	2.36(16) Å	2.2(3) Å	2.30(7) Å
RE-H16_b	2.36(8) Å	2.2(4) Å	2.3(4) Å
Angle			
B1-RE-B2	117(4)°	112(4)°	104(3)°
B1-RE-B3	98(3)°	106(3)°	112(3)°
B1-RE-B4	112(3)°	116(3)°	111(3)°
B2-RE-B3	114(3)°	116(4)°	107(3)°
B2-RE-B4	105(3)°	109(3)°	114(3)°
B3-RE-B4	112(3)°	97(3)°	107(3)°

S2. Magnetic measurements

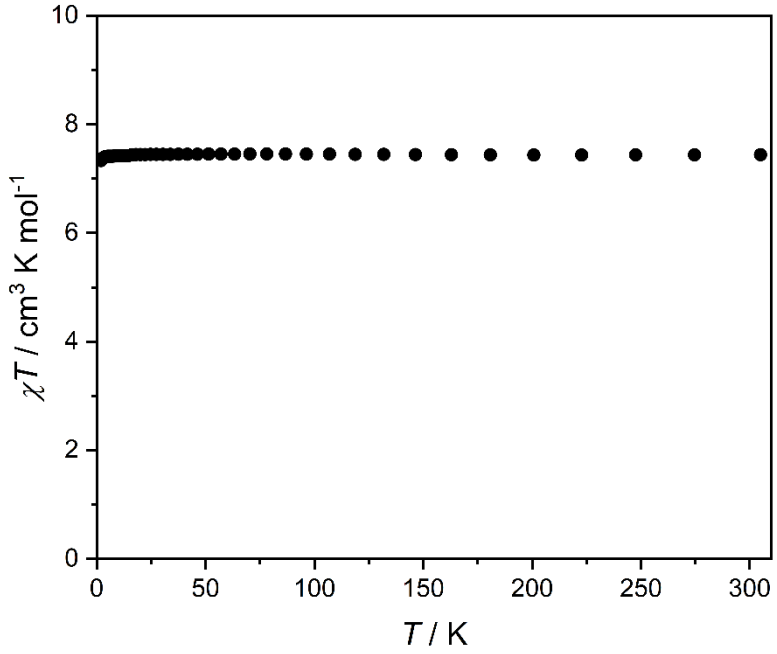

Figure S4. $\chi T(T)$ curve recorded under H_{dc} = 1000 Oe for **1**.

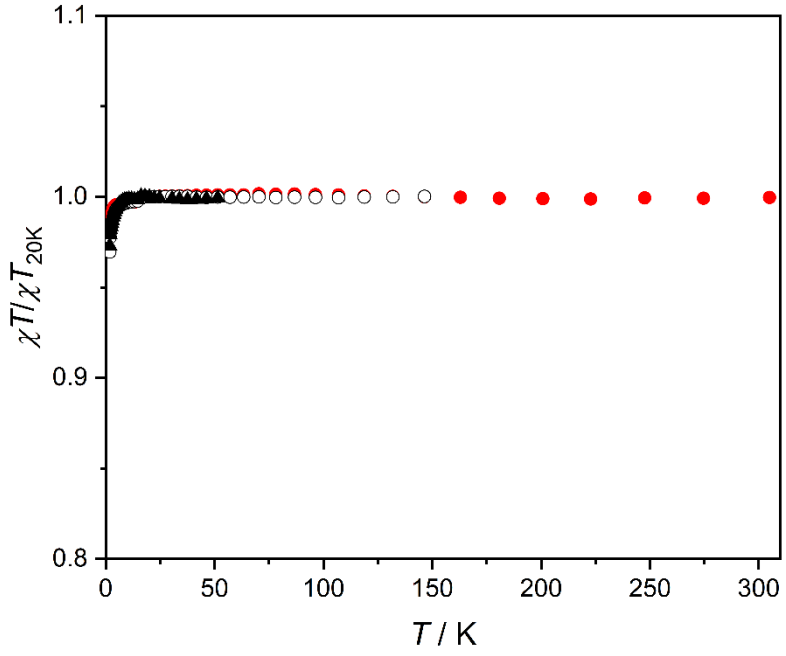

Figure S5. $\chi T(T)$ curves recorded under H_{dc} = 1000 Oe for **1** (red full circles), **2** (open circles) and **3** (black triangles). The χT values for all compounds were divided by the χT value at 20 K, to allow their direct comparison.

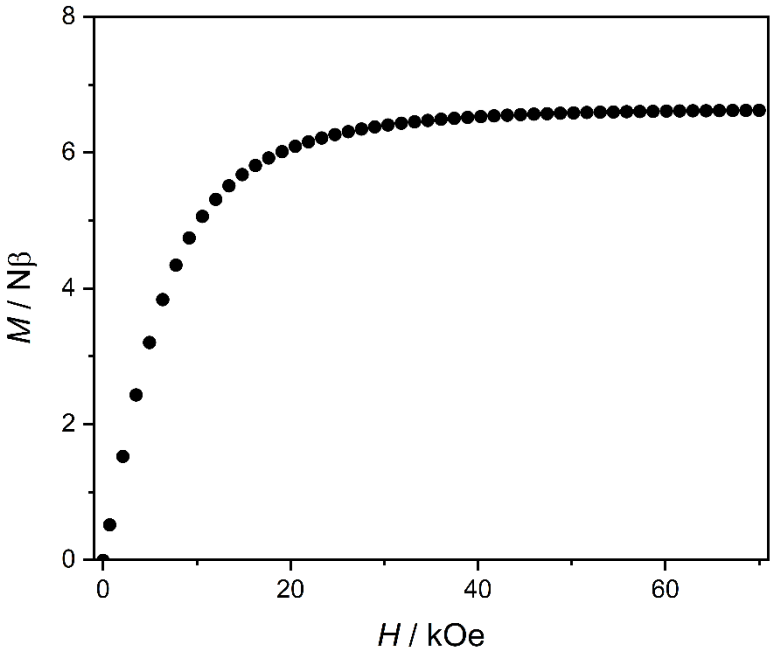

Figure S6. *M*(*H*) curve at *T* = 1.8 K for **1**.

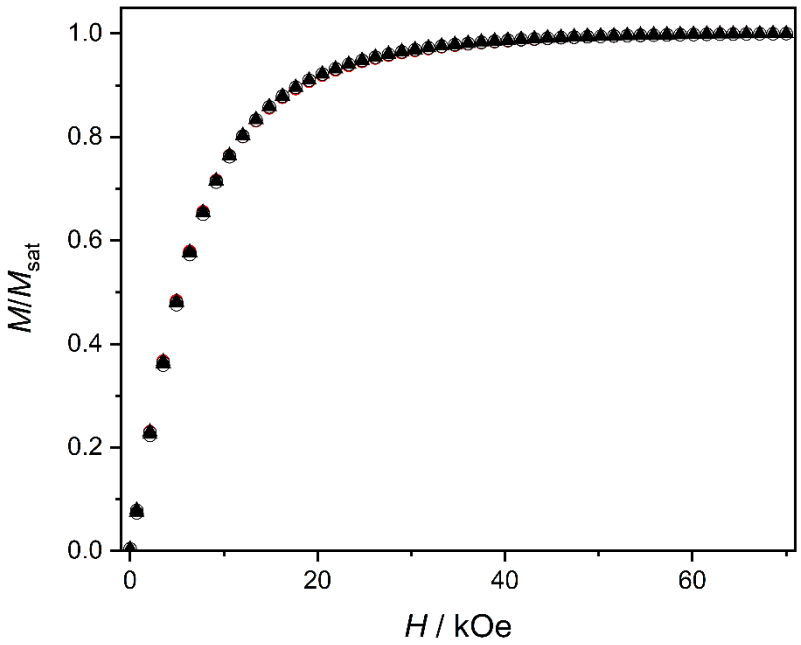

Figure S7. *M*(*H*) curves at *T* = 1.8 K for **1** (black circles), **2** (open circles) and **3** (black triangles). The magnetisation values for all compounds were divided by the magnetisation value at saturation (at 70 kOe), to allow their direct comparison.

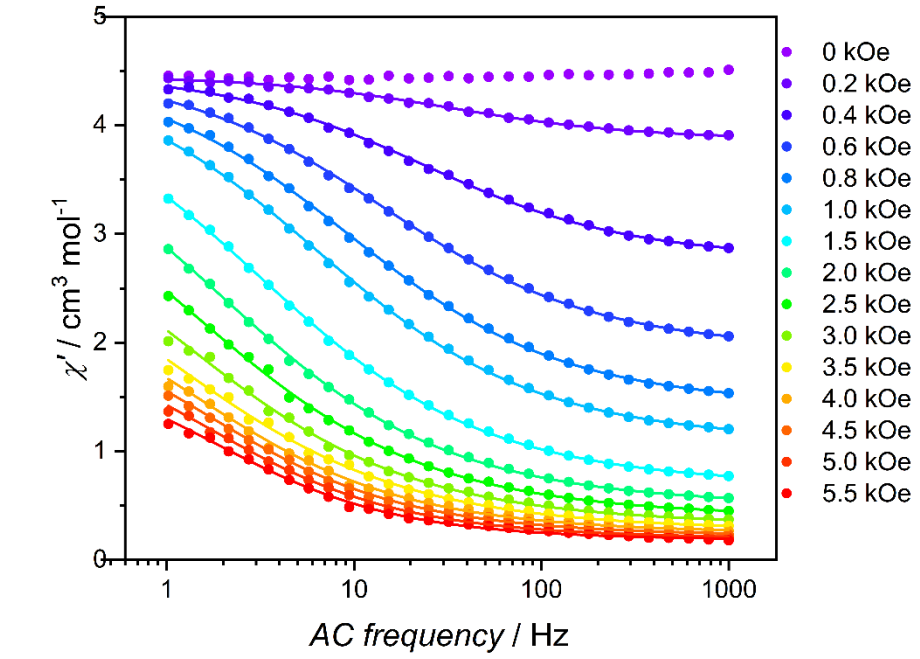

Figure S8. Frequency dependence of χ' recorded at H_{dc} = 0-5500 Oe range for **1** at T = 1.8 K. Solid lines present the best fits to the generalised Debye model.

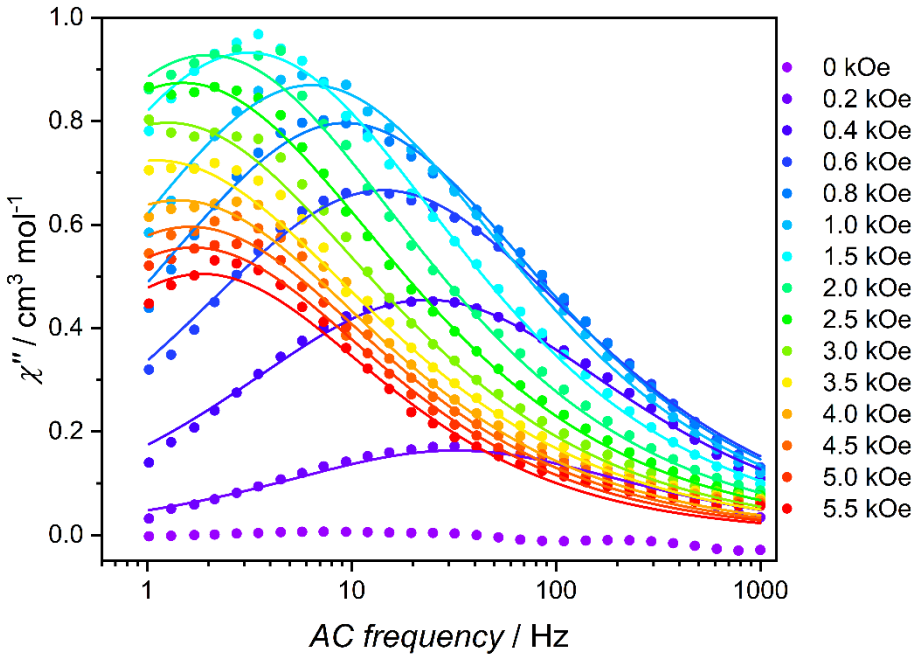

Figure S9. Frequency dependence of χ'' recorded at H_{dc} = 0-5500 Oe range for **1** at T = 1.8 K. Solid lines present the best fits to the generalised Debye model.

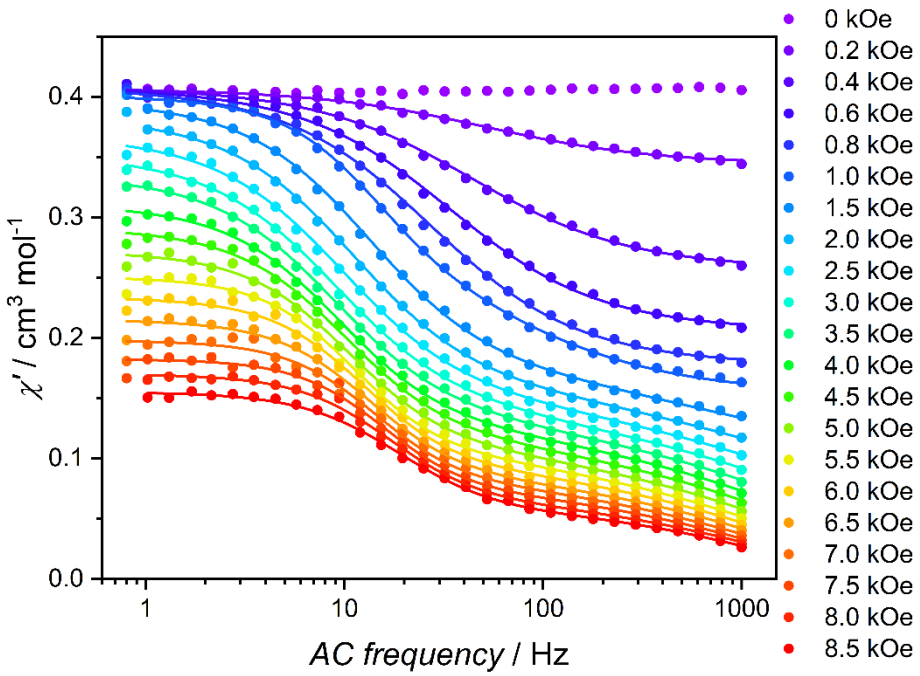

Figure S10. Frequency dependence of χ' recorded at H_{dc} = 0-9000 Oe range for **2** at T = 1.8 K. Solid lines present the best fits to the generalised Debye model.

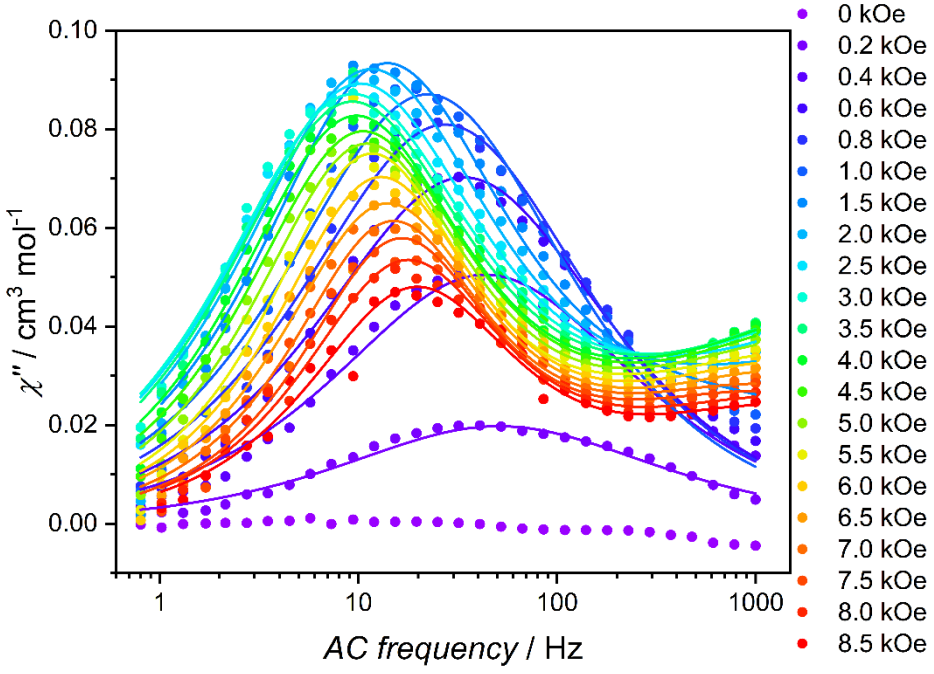

Figure S11. Frequency dependence of χ'' recorded at H_{dc} = 0-9000 Oe range for **2** at T = 1.8 K. Solid lines present the best fits to the generalised Debye model.

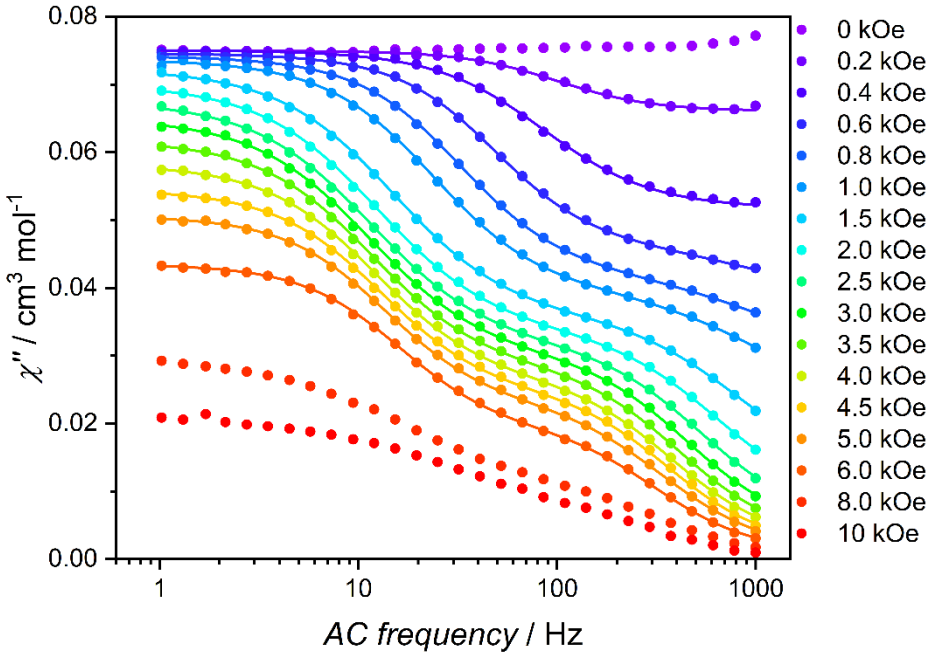

Figure S12. Frequency dependence of χ' recorded at H_{dc} = 0-10000 Oe range for **3** at T = 1.8 K. Solid lines present the best fits to the generalised Debye model.

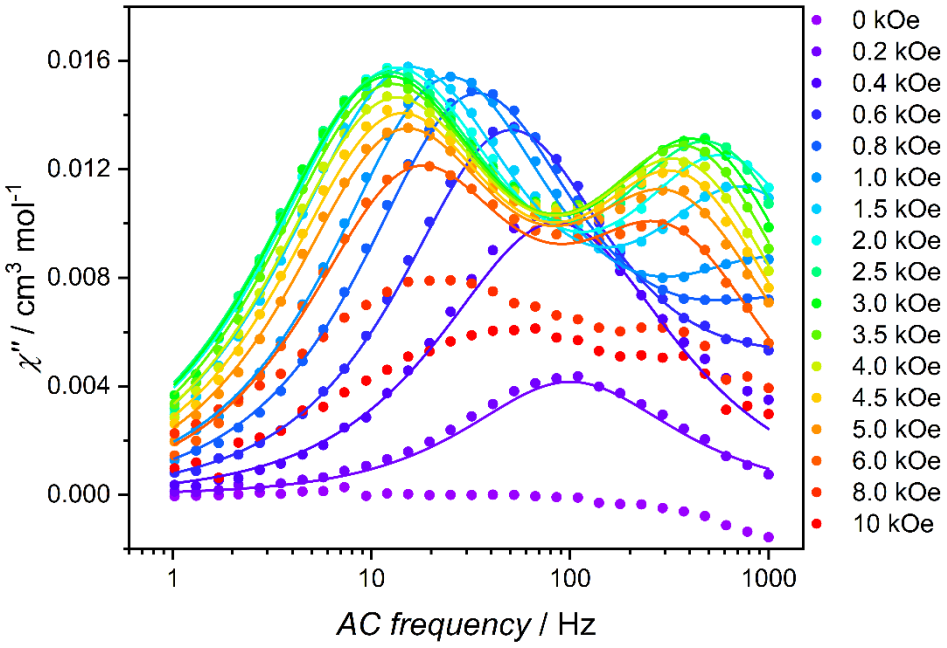

Figure S13. Frequency dependence of χ'' recorded at H_{dc} = 0-10000 Oe range for **3** at T = 1.8 K. Solid lines present the best fits to the generalised Debye model.

Table S4. Fit parameters obtained from *ac* magnetic measurements for **1**-**3** at 1.8 K.*

Compound	**1**	**2**	**3**
A_1 / s^{-1} Oe^{-2}	3.5(2)E-7	1.20(3)E-6	1.9(5)E-6
A_2 / s^{-1}	250(7)	346(5)	791(54)
A_3 / Oe^{-2}	0 (fixed)	1.6(1)E-7	2.1(8)E-7
A_4 / Oe^{-2}	5.1(3)E-6	1.98(9)E-6	5.0(8)E-6
R^2	0.99684	0.99822	0.98296

*assuming $\tau^{-1}(H) = A_1H^2 + A_2(1+ A_3H^2)/(1+A_4H^2)$

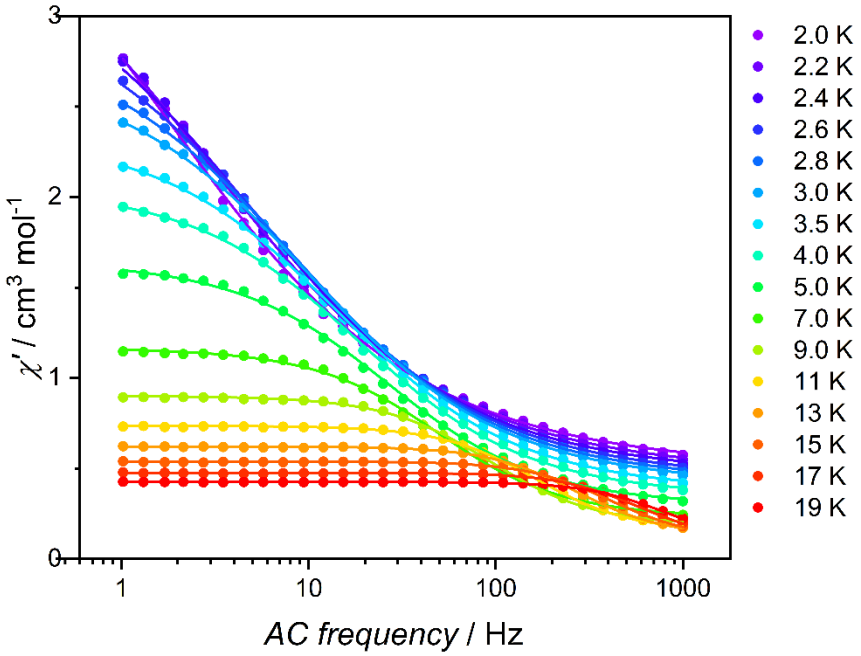

Figure S14. Frequency dependence of χ' recorded at H_{dc} = 2000 Oe for **1**. Solid lines present the best fits to the generalised Debye model.

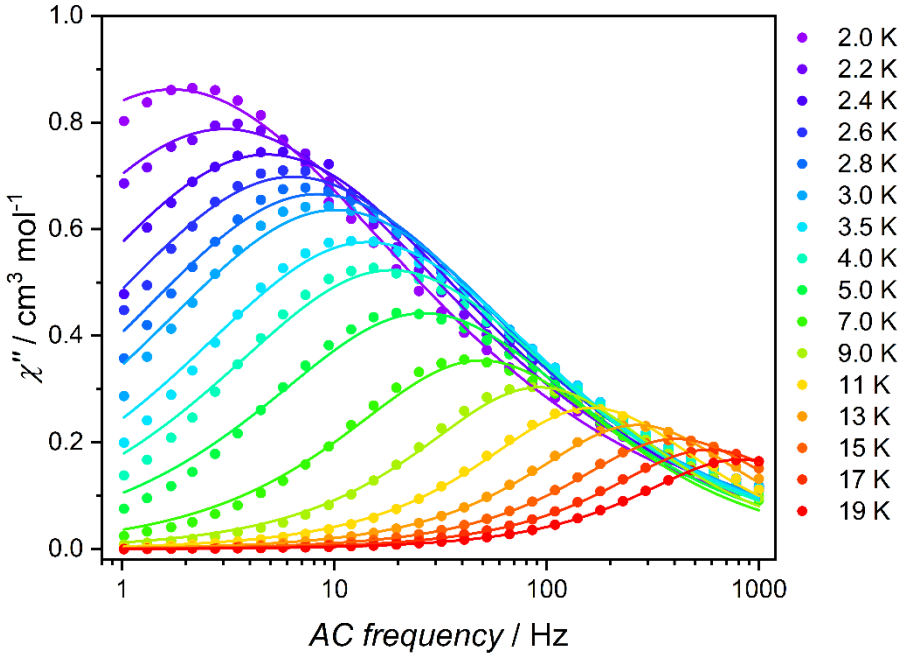

Figure S15. Frequency dependence of χ'' recorded at H_{dc} = 2000 Oe for **1**. Solid lines present the best fits to the generalised Debye model.

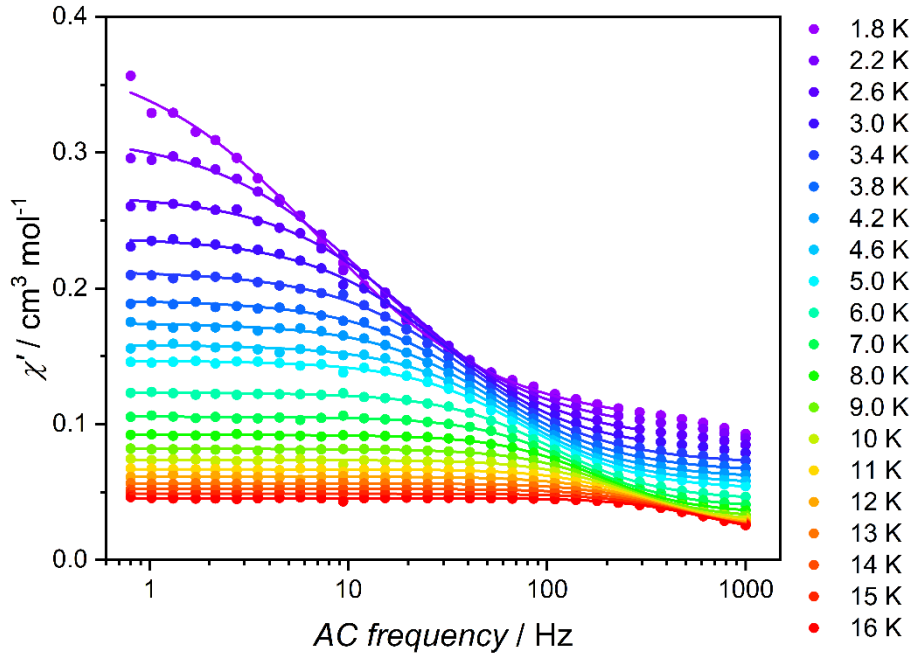

Figure S16. Frequency dependence of χ' recorded at H_{dc} = 2500 Oe for **2**. Solid lines present the best fits to the generalized Debye model.

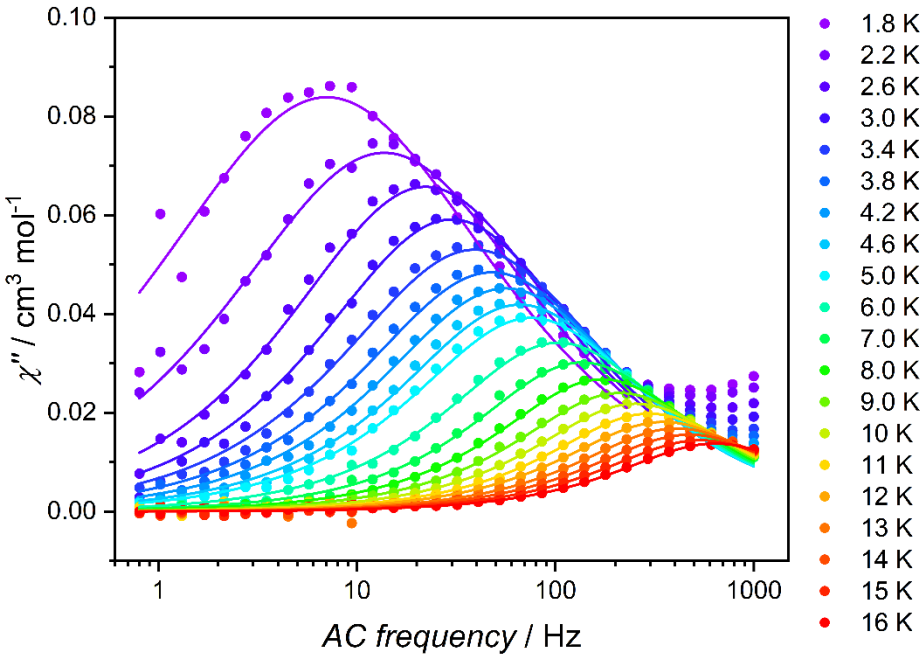

Figure S17. Frequency dependence of χ'' recorded at H_{dc} = 2500 Oe for **2**. Solid lines present the best fits to the generalized Debye model.

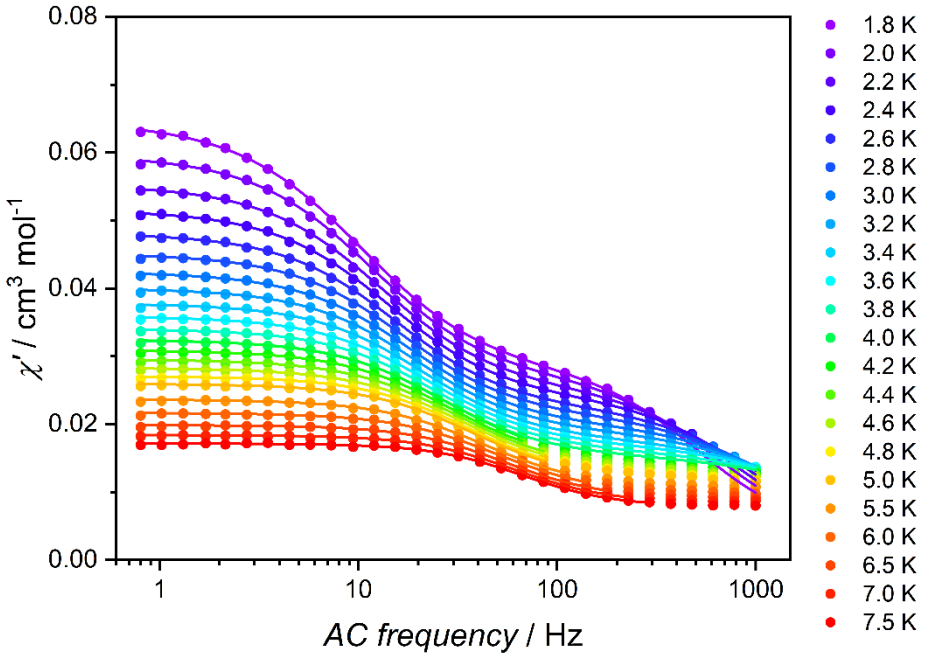

Figure S18. Frequency dependence of χ' recorded at H_{dc} = 3000 Oe for **3** in the 1.8-7.5 K range. Solid lines present the best fits to the generalised Debye model.

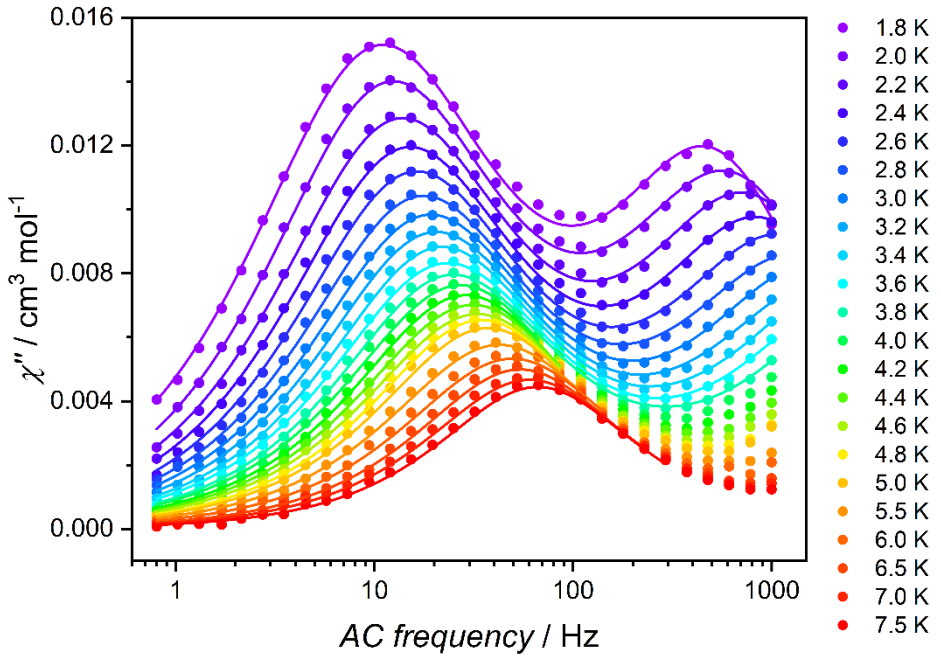

Figure S19. Frequency dependence of χ'' recorded at H_{dc} = 3000 Oe for **3** in the 1.8-7.5 K range. Solid lines present the best fits to the generalised Debye model.

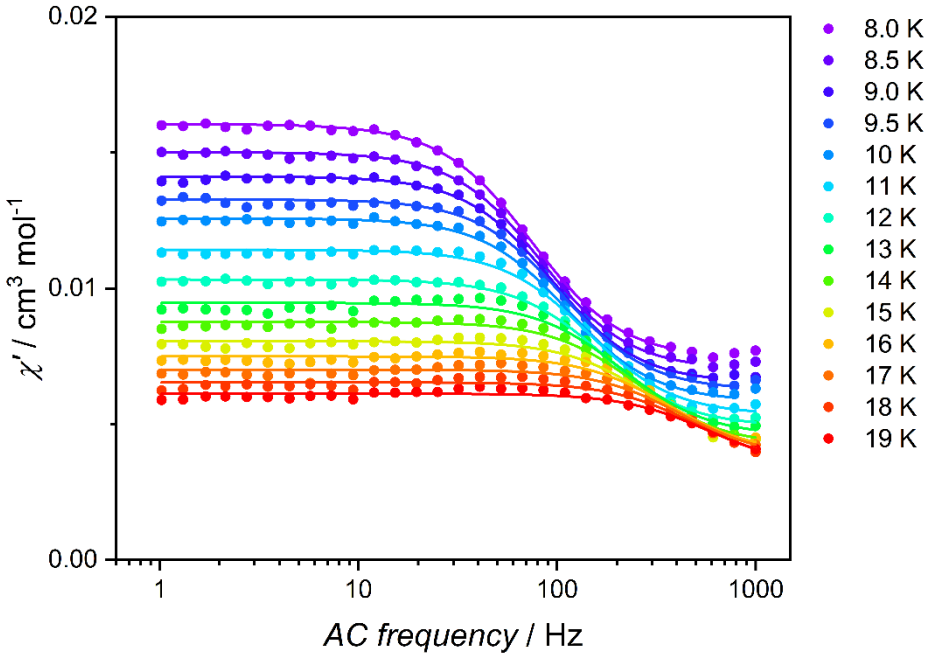

Figure S20. Frequency dependence of χ' recorded at H_{dc} = 3000 Oe for **3** in the 8-19 K range. Solid lines present the best fits to the generalised Debye model.

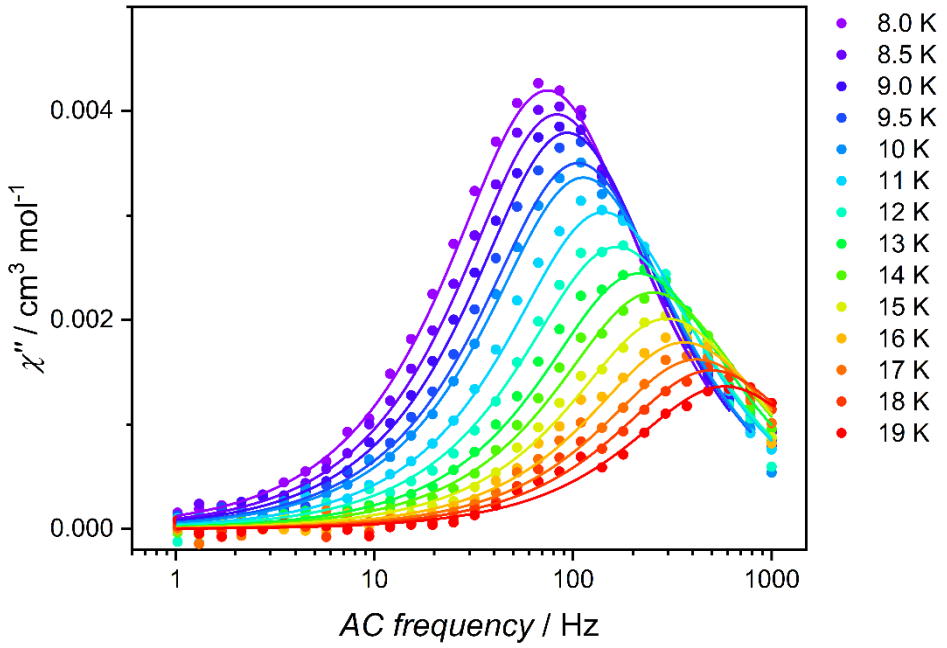

Figure S21. Frequency dependence of χ'' recorded at H_{dc} = 3000 Oe for **3** in the 8-19 K range. Solid lines present the best fits to the generalised Debye model.

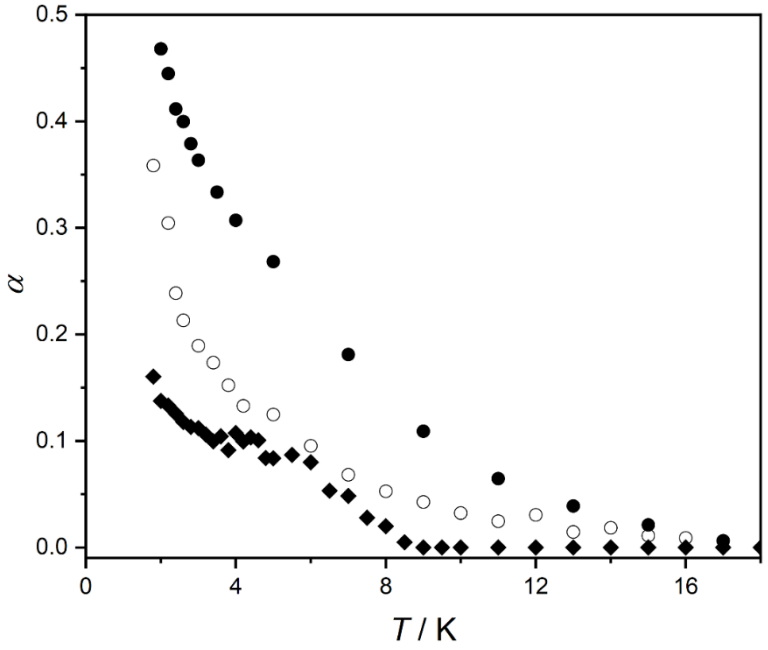

Figure S22. Thermal dependence of *α* derived from *ac* susceptibility measurements for **1** (black circles), **2** (open circles) and **3** (black rhombi).

Table S5. Fit parameters obtained from *ac* magnetic measurements for **1**-**3** at 2000, 2500 and 3000 Oe, respectively.*

Compound	**1**	**2**	**3**
B / s^{-1}	11.7 (fixed)	52.5 (fixed)	50.6 (fixed)
C / s^{-1} K^{-n}	0.88(6)	16(1)	1.05(10)
n	2.94(3)	1.95(3)	2.74(3)
D / s^{-1} K^{-1}	0.78 (fixed)	4.17 (fixed)	9.4 (fixed)
R^2	0.99973	0.99835	0.99835

*assuming $\tau^{-1}(T) = B + CT^n + DT$

Bibliography:

1 W. Wegner, J. J. Zakrzewski, M. Zychowicz and S. Chorazy, *Sci. Reports 2021 111*, 2021, **11**, 1–13.

2 T. Jaroń, W. Wegner, M. K. Cyrański, Dobrzycki and W. Grochala, *J. Solid State Chem.*, 2012, **191**, 279–282.

3 W. Wegner and T. Jaroń, *Mater. 2021, Vol. 14, Page 1329*, 2021, **14**, 1329.

4 R. D. Shannon, *Acta Crystallogr. Sect. A*, 1976, **32**, 751–767.